

## A Spectral, Morphological, and Emission Analysis of Gamma Ray Source HAWC J2031+415

---

Ian Herzog<sup>a,\*</sup>

<sup>a</sup>Michigan State University

E-mail: [herzogia@msu.edu](mailto:herzogia@msu.edu)

The Cygnus Cocoon region is a complex region that contains an OB star cluster that is prominent in the TeV energy range. First observed by HEGRA as the unassociated TeV source TeV J2032+4130, follow-up observations with the High-Altitude Water Cherenkov (HAWC) observatory revealed additional complexity in the region. Previous work has found two sources: 3HWC J2031+415 and 3HWC J2020+403. 3HWC J2031+415 is a significant TeV gamma-ray source whose emission is a composition of 2 sources: HAWC J2030+409, associated with the Fermi-LAT Cocoon and HAWC J2031+415, a pulsar wind nebula (PWN) possibly associated with PSR J2032+4127. 3HWC J2020+403 is a single source and is associated with the supernova remnant Gamma Cygni. Using a multi-source fitting algorithm in The Multi-Mission Maximum Likelihood framework, an investigation of the TeV spectrum and very-high-energy morphology of HAWC J2031+415 is presented in this work. Additionally, X-ray observations from Suzaku are used to constrain the leptonic production of gamma rays by the PWN.

38th International Cosmic Ray Conference (ICRC2023)  
26 July - 3 August, 2023  
Nagoya, Japan



---

\*Speaker

## 1. Introduction

TeV J2032+4130 was first discovered in 2005 by the High-Energy Gamma Ray Astronomy (HEGRA) experiment and was unique in that no lower energy counterpart was associated with it [8]. The source had a measured extent of  $0.11^\circ$  and its spectrum, described with a simple power law, extended to 10 TeV with a power law spectral fit.

Shortly after TeV J2032+4130's discovery, follow-up observations by the X-ray observatories Suzaku and XMM-Newton [9, 10] revealed faint diffuse X-ray emission across the approximate extent of TeV J2032+4130. For the former, they took a measurement across TeV J2032+4130's extent while for the latter they natively found emission approximately the same size as TeV J2032+4130. Additionally, radio observations from the Very Large Array (VLA) also found faint non-thermal emission within TeV J2032+4130's extent [12].

In the third catalog released by the High-Altitude Water Cherenkov (HAWC) observatory, TeV J2032+4130 was labeled as 3HWC J2031+415 [2]. A recent paper by the HAWC collaboration [5] discovered that 3HWC J2031+415 was a composite source whose components were named HAWC J2031+415 and HAWC J2030+409. HAWC J2030+409 was found to be the TeV extension of the *Fermi-LAT* Cygnus Cocoon [11] and was measured as a large  $2.2^\circ$  extended source. HAWC J2031+415 had no known association. This proceeding and corresponding talk assert that HAWC J2031+415 is most probably a pulsar wind nebula (PWN) that is powered by PSR J2032+4127.

## 2. HAWC

The HAWC observatory is a wide-field TeV  $\gamma$ -ray observatory located on the dormant volcano Sierra Negra in Mexico at an elevation of 4100 meters [2]. It is composed of 2 separate arrays: the main array with 300 large water Cherenkov tanks that covers an effective area of approximately 22,000 m<sup>2</sup> and a secondary array of 345 smaller tanks that increases the effective area to about 100,000 m<sup>2</sup>. The primary array tanks each contain 4 photomultiplier tubes (PMTs), one 10 inch at the center of the tank and three 8 inch PMTs surrounding it. The secondary array, known as the outriggers, each contain one 8 inch PMT. While the outriggers do not formally contribute to HAWC's data collection yet, when they do they are anticipated to greatly increase sensitivity to  $> 10$  TeV events.

Once collected, the data is reconstructed using three different algorithms: fractional hit ( $f_{hit}$ ), ground parameter (GP), and an artificial neural network (NN). The  $f_{hit}$  estimator is the most basic and reconstructs the shower energy by using the estimated shower core and the percent of the array triggered by an event [17]. The percentage is binned into one of 11 bins whose definitions are given in Table 1. If an event with energy greater than 30 TeV occurs, the whole array is saturated and  $f_{hit}$  is no longer a valid estimator.

To reconstruct these events, the GP and NN use complex reconstruction techniques to accurately estimate the energies of the parent  $\gamma$ -rays [4]. The GP estimator reconstructs the shower energy by using the shower density measured at 40 meters away from the shower core. The NN utilizes a double layer neural network that takes 3 broad parameters as inputs: the amount of energy deposited, the amount of the shower contained within the HAWC main array footprint, and the attenuation degree caused by the atmosphere. Both energy estimators sub-divide each  $f_{hit}$  bin into 12 sub-bins

Bin	Low fraction hit	High fraction hit
0	0.027	0.047
1	0.047	0.07
2	0.07	0.11
3	0.11	0.16
4	0.16	0.25
5	0.25	0.37
6	0.37	0.51
7	0.51	0.66
8	0.66	0.78
9	0.78	0.88
10	0.88	1.0

**Table 1:** The  $f_{hit}$  binning scheme. Each bin is based solely on the percentage of the array triggered by a shower

Bin	Energy Range (TeV)
a	0.316 - 0.562
b	0.562 - 1.0
c	1.0 - 1.78
d	1.78 - 3.16
e	3.16 - 5.62
f	5.62 - 10.0
g	10.0 - 17.8
h	17.8 - 31.6
i	31.6 - 56.2
j	56.2 - 100
k	100 - 177
l	177 - 316

**Table 2:** GP and NN energy estimator bins. Each  $f_{hit}$  bin is composed of 12 energy estimator bins

and whose definitions are given in Table 2. It should be noted that not all bins are populated as the probability of having a reconstructed shower having an estimated energy of  $> 177$  TeV trigger only two percent of array; this would be bin 0l and is excluded from this fit.

### 3. Methodology

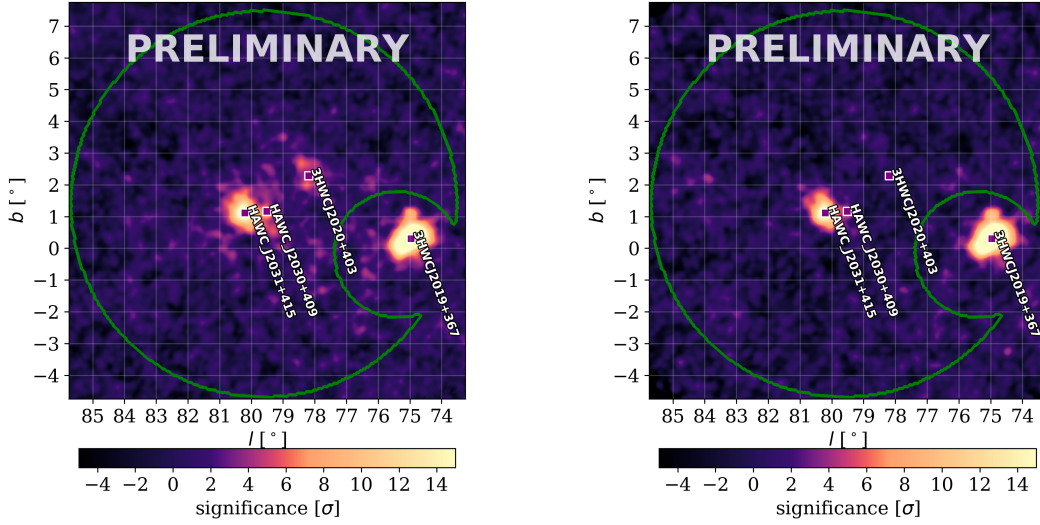
#### 3.1 Spectral Analysis

The Region of Interest (ROI) considered for this analysis is a circular region centered at RA =  $306.456^\circ$ , Dec =  $40.731^\circ$  with a  $6^\circ$  radius. The initial data set is shown in Figure 1a. To determine the number of sources in the ROI, a systematic source search inspired by [1] is used. This search utilizes the Multi-Mission Maximum Likelihood (3ML) framework [13]. The framework considers the Test Statistic (TS) which is useful to quantify the significance in model improvement when comparing two models. The TS is defined by considered two hypotheses: an alternate and null hypothesis by

$$TS = 2 \ln \frac{L_{alt}}{L_{null}} \quad (1)$$

If two alternate hypotheses are considered, then the  $\Delta TS = 2 \ln(L_2/L_1)$  can be used to compare between them. For this study,  $\Delta TS > 25$  is considered strong evidence for an alternate model. The source search starts by applying a diffuse background emission (DBE) model that handles both the galactic diffuse emission along with any unresolved sources within the ROI. Then a point source (PS) with floating location and a simple power law spectral model is added to the ROI and is fitted. The spectral shape of this source is assumed to be given by

$$\frac{dN}{dE} = N_o \left( \frac{E}{E_p} \right)^{-\gamma} \quad (2)$$



(a) Initial ROI with the source associations found from the (b) HAWC J2031+415 isolated after all other emission has systematic source search method. Emission from 3HWC been subtracted out. J2019+367 is excluded from the fit with a mask.

where  $N_o$  is the flux normalization,  $\gamma$  is the index, and  $E_p$  is the pivot energy and is used to de-correlate the flux normalization and index for the source. If the  $\Delta TS > 25$ , then the point source model is preferred over the other alternate hypothesis (DBE only model). Then another PS is fitted to the ROI and this process repeats until the  $\Delta TS < 25$  threshold is reached. Each PS has a power law spectral model; more complex models are considered later.

Once PS stop being added to the ROI, an extension test can take place. Each PS has their locations fixed and the highest TS one is converted to a symmetric 2D Gaussian with width  $\sigma$  extended (EXT) source. The ROI is fitted again and every PS whose TS drops below 25 is dropped. It should be noted that if  $\Delta TS < 25$  from the extension test, then the extended source is converted back to a PS. Then the next brightest PS is converted to an EXT and so on. Once the extension test completes, all locations are freed and the ROI is fitted once more.

With the number of sources and their morphologies found, the spectrum for each source is found. This is done by calculating the Bayesian Information Criterion (BIC) where a  $BIC > 2$  for  $L_1 - L_2$  (from the above hypotheses) indicates that  $L_2$  is preferred. Three spectral models are considered: a power law (PL), log parabola (LP), and a power law with exponential cut-off (PLC). The latter two are given below

$$\frac{dN}{dE} = N_o \left( \frac{E}{E_p} \right)^{-\gamma - \beta \ln(E/E_p)} \quad (3)$$

$$\frac{dN}{dE} = N_o \left( \frac{E}{E_p} \right)^{-\gamma} \exp\left(-\frac{E}{E_c}\right) \quad (4)$$

Source	R.A [deg]	Dec. [deg]	Morphology [deg]	Model
3HWC J2020+403	305.00 $\pm$ 0.03	40.49 $\pm$ 0.02	0.63 (fixed)	PL
HAWC J2030+409	307.96 $\pm$ 0.10	40.93 $\pm$ 0.02	2.20 $\pm$ 0.20	LP
HAWC J2031+415	307.96 $\pm$ 0.02	41.48 $\pm$ 0.02	0.26 $\pm$ 0.02	PLC

**Table 3:** The sources considered with location, morphology, and their associated counterparts [4, 6]

The new terms  $\beta$  and  $E_c$  are the curvature of the spectrum decay and cut-off energy respectively. The results are given in Table 3.

The morphology of 3HWC J2020+403 was previously found [5, 14] to be an extended disk model with a fixed radius of  $0.63^\circ$ . A disk model differs from a 2D Gaussian by the way the flux is emitted from the source; for a disk model, the flux is constant across the whole region while for an extended source (EXT), the emitted flux decays radially. All sources were tested with a disk model and only 3HWC J2020+403 was preferred having one, the other two remain EXT.

### 3.2 Energy Morphology Study

With the ROI properly modelled, an energy morphology study can be completed. The emission from HAWC J2031+415 is isolated by fixing the other two sources and the DBE to their best-fit parameters and subtracted from the data set, as shown in Figure 1b. The energy morphology study performed follows the format outlined in [6, 15] and is discussed in some detail below.

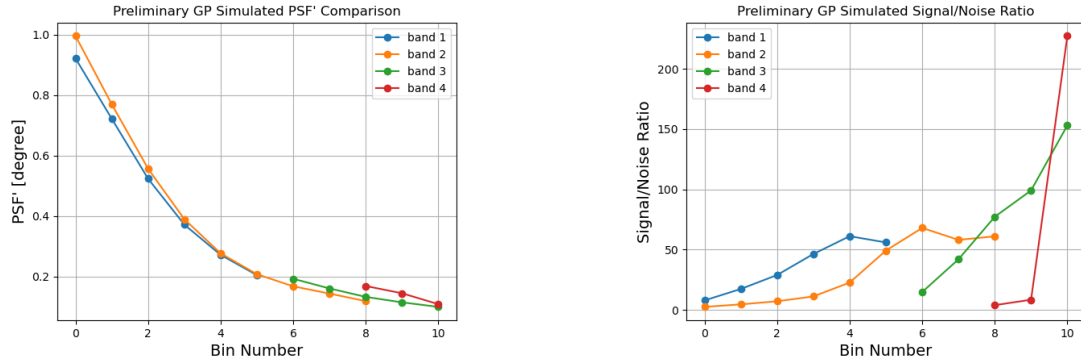
The GP energy estimator bins are divided into four bands: 0.3 - 1.8 (a,b,c), 1.8 - 10 (d,e,f), 10 - 56 (g,h,i), and 56 - 316 (j,k,l) TeV. There is not enough data in the bands 1 and 4 to perform a dedicated fit with 3ML. As such, a slicing and counting method is used instead. This method defines a rectangular region centered on the source and divides the region into a series of sub-bins. Each sub-bin has its excess counts summed, plotted, and the resulting shape has a 1D Gaussian (henceforth referred to as PSF') fitted to it. The selected rectangle has a length of  $6^\circ$  with a width of  $1^\circ$  and 50 sub-bins.

As mentioned, not all energy bins have sufficient data to meaningfully contribute to the fit. As such, a series of systematic tests are used to select the bins while maintaining the best possible signal to noise ratio. Three tests are performed: real data vs simulated data at the same declination for a bright source (also used for bin selection), real data vs simulated data of a source near HAWC J2031+415's declination, and lastly a comparison between simulated sources at different declinations. Only the first test results in significant systematic uncertainty and is discussed below.

The source used for comparison is the Crab Nebula, the brightest source in HAWC's field of view. The source is fitted with a simple PS PL model and then is simulated using those best fit parameters at the Crab's location. Then both the real and simulated data have the slicing method performed on them and are compared.

With this study completed, the next step is to select the bins that minimize the PSF' while maintaining the highest possible significance in each band. This can be done by combining each available energy bin to their respective  $f_{hit}$  bin. For example, band 1  $f_{hit}$  bin 3 might have energy bins a, b, and c and all three get combined into one bin when considering its PSF' and signal to noise (S/N) or significance ratio. This is shown in Figure 2.

As shown in Figure 2, the PSF' of the bins continuously decreases while the S/N follows a parabolic shape. Therefore, the following criteria is used for bin selection: the  $f_{hit}$  with the best S/N for each energy band is selected along with all bins following it. For bins before the highest S/N one, they are selected if their PSF' is within approximately 25% of the highest S/N one. This results in  $f_{hit}$  bins 3 4 5 selected for band 1, bins 5 6 7 8 for band 2, bins 8 9 10 for band 3, and bins 8 9 10 for band 4.



(a) Comparing PSF' of each combined  $f_{hit}$  bin of each energy band

(b) Comparing the S/N ratio of each combined  $f_{hit}$  bin of each energy band.

**Figure 2:** Determining the best bins to keep for each energy band. Each band is color-coded and corresponds to their respective energy intervals.

The fit results can be broken into two categories: hard and soft fits. Bands 2 and 3 are hard fits with significant excess emission observed and clear fits. Bands 1 and 4 are soft fits where there is little to no emission observed and poor fits. These are shown in the corresponding presentation. Additionally, there is no clear energy-dependent morphology observed.

#### 4. Multi-Wavelength Analysis

The multi-wavelength analysis of HAWC J2031+415 utilizes the NAIMA framework [18]. This framework models non-thermal emission using a wide range of energy using Markov chain Monte Carlo calculations. The data considered is given as such: the HAWC flux points, TeV flux points from a VERITAS observation [7], X-ray observations from Suzaku [10] and XMM-Newton [9], and radio data from the VLA [12]. The data is well fit by a leptonic model considering synchrotron emission being responsible for the radio and X-ray data with inverse Compton scattering producing the TeV emission. The fit values and plots are presented in the corresponding talk.

#### References

- [1] Abdollahi, Soheila, et al. "Fermi large area telescope fourth source catalog." The Astrophysical Journal Supplement Series 247.1 (2020): 33.
- [2] A. Albert et al "3HWC: The Third HAWC Catalog of Very-high-energy Gamma-Ray Sources" 2020 ApJ 905 76

- [3] Lyne, Andrew & Stappers, Ben & Keith, Michael & Ray, Paul & Kerr, Mônica & Camilo, Fernando & Johnson, Tyrel. (2015). The binary nature of PSR J2032+4127. *Monthly Notices of the Royal Astronomical Society*. 451. 10.1093/mnras/stv236.
- [4] A. U. Abeysekara et al, "Measurement of the Crab Nebula Spectrum Past 100 TeV with HAWC" 2019 *ApJ* 881 134
- [5] Abeysekara, A.U., Albert, A., Alfaro, R. et al. "HAWC observations of the acceleration of very-high-energy cosmic rays in the Cygnus Cocoon." *Nat Astron* 5, 465–471 (2021). <https://doi.org/10.1038/s41550-021-01318-y>
- [6] A. Albert et al, "Spectrum and Morphology of the Very-high-energy Source HAWC J2019+368" 2021 *ApJ* 911 143
- [7] E. Aliu et al, "OBSERVATIONS OF THE UNIDENTIFIED GAMMA-RAY SOURCE TeV J2032+4130 BY VERITAS" 2014 *ApJ* 783 16
- [8] Aharonian, F. et al. "The unidentified TeV source (TeV J2032+4130) and surrounding field" 224 *Final HEGRA IACT-System results. Astron. Astrophys.* 431, 197-202 (2005)
- [9] Horns, D., et al. "XMM-Newton observations of the first unidentified TeV gamma-ray source TeV J2032+ 4130." *Astronomy and Astrophysics* 469.1 (2007): L17-L21.
- [10] Murakami, Hiroshi, et al. "Detection of X-ray emission from the unidentified TeV Gamma-ray source TeV J2032+ 4130." *Publications of the Astronomical Society of Japan* 63.sp3 (2011): S873-S878.
- [11] Ackermann, Markus, et al. "A cocoon of freshly accelerated cosmic rays detected by Fermi in the Cygnus superbubble." *science* 334.6059 (2011): 1103-1107.
- [12] Paredes, Josep M., et al. "The population of radio sources in the field of the unidentified gamma-ray source TeV J2032+ 4130." *The Astrophysical Journal* 654.2 (2006): L135.
- [13] Vianello, G., et al. 2015, 34th ICRC, PoS, 1042
- [14] Fleischhack, H. for the HAWC collaboration. PoS(ICRC2019)675
- [15] Joshi, V. "Reconstruction and Analysis of Highest Energy gamma-rays and its Application to Pulsar Wind Nebulae", PhD Thesis, Ruperto-Carola University, Germany (2019)
- [16] Cao, Z., Aharonian, F.A., An, Q. et al. Ultrahigh-energy photons up to 1.4 petaelectronvolts from 12  $\gamma$ -ray Galactic sources. *Nature* 594, 33–36 (2021). <https://doi.org/10.1038/s41586-021-03498-z>
- [17] Abeysekara, A. U., et al. "Observation of the crab nebula with the HAWC gamma-ray observatory." *The Astrophysical Journal* 843.1 (2017): 39.
- [18] Zabalza, Víctor. "naima: a Python package for inference of relativistic particle energy distributions from observed nonthermal spectra." *arXiv preprint arXiv:1509.03319* (2015).

## Full Authors List: Collaboration

**Note comment afterwards:** Collaborations have the possibility to provide an authors list in xml format which will be used while generating the DOI entries making the full authors list searchable in databases like Inspire HEP.

A. Albert<sup>1</sup>, R. Alfaro<sup>2</sup>, C. Alvarez<sup>3</sup>, A. Andrés<sup>4</sup>, J.C. Arteaga-Velázquez<sup>5</sup>, D. Avila Rojas<sup>2</sup>, H.A. Ayala Solares<sup>6</sup>, R. Babu<sup>7</sup>, E. Belmont-Moreno<sup>2</sup>, K.S. Caballero-Mora<sup>3</sup>, T. Capistrán<sup>4</sup>, S. Yun-Cárcamo<sup>8</sup>, A. Carramiñana<sup>9</sup>, F. Carreón<sup>4</sup>, U. Cotti<sup>5</sup>, J. Cotzomi<sup>26</sup>, S. Coutiño de León<sup>10</sup>, E. De la Fuente<sup>11</sup>, D. Depaoli<sup>12</sup>, C. de León<sup>5</sup>, R. Diaz Hernandez<sup>9</sup>, J.C. Díaz-Vélez<sup>11</sup>, B.L. Dingus<sup>1</sup>, M. Durocher<sup>1</sup>, M.A. DuVernois<sup>10</sup>, K. Engel<sup>8</sup>, C. Espinoza<sup>2</sup>, K.L. Fan<sup>8</sup>, K. Fang<sup>10</sup>, N.I. Fraija<sup>4</sup>, J.A. García-González<sup>13</sup>, F. Garfías<sup>4</sup>, H. Goksu<sup>12</sup>, M.M. González<sup>4</sup>, J.A. Goodman<sup>8</sup>, S. Groetsch<sup>7</sup>, J.P. Harding<sup>1</sup>, S. Hernandez<sup>2</sup>, I. Herzog<sup>14</sup>, J. Hinton<sup>12</sup>, D. Huang<sup>7</sup>, F. Hueyotl-Zahuantitla<sup>3</sup>, P. Hüntemeyer<sup>7</sup>, A. Iriarte<sup>4</sup>, V. Joshi<sup>28</sup>, S. Kaufmann<sup>15</sup>, D. Kieda<sup>16</sup>, A. Lara<sup>17</sup>, J. Lee<sup>18</sup>, W.H. Lee<sup>4</sup>, H. León Vargas<sup>2</sup>, J. Linnemann<sup>14</sup>, A.L. Longinotti<sup>4</sup>, G. Luis-Raya<sup>15</sup>, K. Malone<sup>19</sup>, J. Martínez-Castro<sup>20</sup>, J.A.J. Matthews<sup>21</sup>, P. Miranda-Romagnoli<sup>22</sup>, J. Montes<sup>4</sup>, J.A. Morales-Soto<sup>5</sup>, M. Mostafá<sup>6</sup>, L. Nellen<sup>23</sup>, M.U. Nisa<sup>14</sup>, R. Noriega-Papaqui<sup>22</sup>, L. Olivera-Nieto<sup>12</sup>, N. Omodei<sup>24</sup>, Y. Pérez Araujo<sup>4</sup>, E.G. Pérez-Pérez<sup>15</sup>, A. Pratts<sup>2</sup>, C.D. Rho<sup>25</sup>, D. Rosa-Gonzalez<sup>9</sup>, E. Ruiz-Velasco<sup>12</sup>, H. Salazar<sup>26</sup>, D. Salazar-Gallegos<sup>14</sup>, A. Sandoval<sup>2</sup>, M. Schneider<sup>8</sup>, G. Schwefer<sup>12</sup>, J. Serna-Franco<sup>2</sup>, A.J. Smith<sup>8</sup>, Y. Son<sup>18</sup>, R.W. Springer<sup>16</sup>, O. Tibolla<sup>15</sup>, K. Tollefson<sup>14</sup>, I. Torres<sup>9</sup>, R. Torres-Escobedo<sup>27</sup>, R. Turner<sup>7</sup>, F. Ureña-Mena<sup>9</sup>, E. Varela<sup>26</sup>, L. Villaseñor<sup>26</sup>, X. Wang<sup>7</sup>, I.J. Watson<sup>18</sup>, F. Werner<sup>12</sup>, K. Whitaker<sup>6</sup>, E. Willox<sup>8</sup>, H. Wu<sup>10</sup>, H. Zhou<sup>27</sup>

<sup>1</sup>Physics Division, Los Alamos National Laboratory, Los Alamos, NM, USA, <sup>2</sup>Instituto de Física, Universidad Nacional Autónoma de México, Ciudad de México, México, <sup>3</sup>Universidad Autónoma de Chiapas, Tuxtla Gutiérrez, Chiapas, México, <sup>4</sup>Instituto de Astronomía, Universidad Nacional Autónoma de México, Ciudad de México, México, <sup>5</sup>Instituto de Física y Matemáticas, Universidad Michoacana de San Nicolás de Hidalgo, Morelia, Michoacán, México, <sup>6</sup>Department of Physics, Pennsylvania State University, University Park, PA, USA, <sup>7</sup>Department of Physics, Michigan Technological University, Houghton, MI, USA, <sup>8</sup>Department of Physics, University of Maryland, College Park, MD, USA, <sup>9</sup>Instituto Nacional de Astrofísica, Óptica y Electrónica, Tonantzintla, Puebla, México, <sup>10</sup>Department of Physics, University of Wisconsin-Madison, Madison, WI, USA, <sup>11</sup>CUCEI, CUCEA, Universidad de Guadalajara, Guadalajara, Jalisco, México, <sup>12</sup>Max-Planck Institute for Nuclear Physics, Heidelberg, Germany, <sup>13</sup>Tecnológico de Monterrey, Escuela de Ingeniería y Ciencias, Ave. Eugenio Garza Sada 2501, Monterrey, N.L., 64849, México, <sup>14</sup>Department of Physics and Astronomy, Michigan State University, East Lansing, MI, USA, <sup>15</sup>Universidad Politécnica de Pachuca, Pachuca, Hgo, México, <sup>16</sup>Department of Physics and Astronomy, University of Utah, Salt Lake City, UT, USA, <sup>17</sup>Instituto de Geofísica, Universidad Nacional Autónoma de México, Ciudad de México, México, <sup>18</sup>University of Seoul, Seoul, Rep. of Korea, <sup>19</sup>Space Science and Applications Group, Los Alamos National Laboratory, Los Alamos, NM USA, <sup>20</sup>Centro de Investigación en Computación, Instituto Politécnico Nacional, Ciudad de México, México, <sup>21</sup>Department of Physics and Astronomy, University of New Mexico, Albuquerque, NM, USA, <sup>22</sup>Universidad Autónoma del Estado de Hidalgo, Pachuca, Hgo., México, <sup>23</sup>Instituto de Ciencias Nucleares, Universidad Nacional Autónoma de México, Ciudad de México, México, <sup>24</sup>Stanford University, Stanford, CA, USA, <sup>25</sup>Department of Physics, Sungkyunkwan University, Suwon, South Korea, <sup>26</sup>Facultad de Ciencias Físico Matemáticas, Benemérita Universidad Autónoma de Puebla, Puebla, México, <sup>27</sup>Tsung-Dao Lee Institute and School of Physics and Astronomy, Shanghai Jiao Tong University, Shanghai, China, <sup>28</sup>Erlangen Centre for Astroparticle Physics, Friedrich Alexander Universität, Erlangen, BY, Germany